Algorithm performance in the determination of the refractive-index profile of optical fibers

Michael R. Hutsel,[1] Carole C. Montarou,[1] Alexi I. Dachevski,[1] and Thomas K. Gaylord[1,*]

School of Electrical and Computer Engineering, Georgia Institute of Technology, 777 Atlantic Drive, N.W., Atlanta, Georgia 30332-0250, USA

*Corresponding author: tgaylord@ece.gatech.edu

Received 25 September 2007; accepted 18 December 2007;
posted 9 January 2008 (Doc. ID 87796); published 20 February 2008

Three algorithms for computing the refractive-index profile of azimuthally symmetric optical fibers via the inverse Abel transform are compared to determine their relative accuracies. Appropriate values of algorithm parameters are also determined. The direct differentiation algorithm, the iterative algorithm, and the Fourier algorithm are used to calculate the refractive-index profile from simulated measurements of the phase shift of light transmitted transversely through the fiber. The rms error in the calculated index profile is used to quantify the accuracy of each algorithm. The Fourier algorithm is typically the most accurate of the three. © 2008 Optical Society of America

OCIS codes: 060.2270, 060.2300.

1. Introduction

As optical fiber technology continues to advance and new fibers and fiber-based devices are introduced, it becomes increasingly important to accurately measure their transmission and physical characteristics. Transmission characteristics such as loss, dispersion, and spectral response are important for determining signal behavior in fibers and fiber-based devices. Physical characteristics such as size, refractive index, and residual stress are important in the modeling, design, and evaluation of fibers and fiber-based devices. While highly developed commercial equipment is available to measure transmission characteristics, many of the techniques for measuring physical characteristics require custom laboratory facilities.

The importance of characterizing refractive index and residual stress has led to the development of many techniques to determine these physical parameters. Common to many of these techniques is the use of an imaging system in which light is transmitted transversely through the fiber. Such a system allows the fiber to be examined nondestructively and can be readily constructed due to the sophistication of modern microscopy and digital imaging equipment. One limitation of this type of system is that direct measurement of the refractive index or residual stress is not possible. Optical measurements obtained from the imaging system must be used to calculate the desired physical parameters. The refractive index and residual stress usually have azimuthal symmetry within the fiber. This allows the physical parameter to be calculated using the inverse Abel transform of the optical measurement. Furthermore, only a single, one-dimensional optical measurement along the radial direction of the fiber is necessary.

To calculate the refractive-index profile of a fiber, the phase shift of light traveling transversely through the fiber must be measured. In an early technique, the phase shift was obtained from the interference fringes generated when the fiber was placed in the sample arm of an interference microscope [1]. In a more recent, noninterferometric technique, called quantitative-phase microscopy, the phase shift was obtained from three transverse images of the fiber: one in-focus and two slightly defocused [2,3]. The refractive index can also be

0003-6935/08/060760-08$15.00/0

calculated from a measurement of the spatial gradient of the phase shift. Measurement of the phase-shift gradient of a fiber has been demonstrated using a variation of the quantitative-phase microscopy technique [4] and differential interference contrast microscopy [5].

To calculate the residual stress present in a fiber, the retardation of light traveling transversely through the fiber must be measured. The first demonstration of measuring the retardation in a fiber utilized a polariscope and the Sénarmont compensation technique [6]. It was shown, however, that this compensation technique is not generally suitable for measuring the small values of retardation found in optical fibers [7]. Subsequent improvements were made with the addition of the half-shade device [8] and with the use of a modified version of the Sénarmont compensation technique [9,10]. Recently, the two-wave-plate compensator method was shown to greatly improve upon the accuracy of the Sénarmont compensation technique for measuring small values of retardation [7,11].

While much work has gone into the development of these measurement techniques and their apparatuses, there has been no detailed study of the various algorithms available to compute the inverse Abel transform of the optical measurements. In this paper, we present a comparison of three algorithms to compute the inverse Abel transform of a phase-shift measurement. The purpose of this comparison is to provide a guide for choosing an appropriate algorithm, along with the various parameters necessary for that algorithm. We have chosen to study the phase-shift, refractive-index relationship due to the availability of mathematical models for these parameters. The methods presented also provide a platform for evaluating algorithm performance in computing the residual stress from retardation measurements.

The Abel transform relationship between the phase shift and the refractive index is presented in Section 2, along with the various algorithms to compute the inverse Abel transform. In Section 3, the mathematical models of the refractive index and phase shift are given, and the variable parameters for each algorithm are discussed. The performance of each algorithm in computing the refractive index is presented in Section 4. Finally, the most appropriate algorithm and its advantages and disadvantages are summarized in Section 5.

2. Theory

In optical fibers, the Abel transform relates the phase shift of light traveling transversely through the fiber, $\phi(y)$, to the relative refractive index of the fiber, $\Delta n(r)$. The phase shift is given by the forward Abel transform of the relative refractive index

$$\phi(y) = \frac{4\pi}{\lambda}\int_r^\infty \Delta n(r)\frac{r}{\sqrt{r^2 - y^2}}\mathrm{d}r, \tag{1}$$

where y and r both correspond to the radial distance from the longitudinal fiber axis. The use of two separate symbols is necessary for both mathematical and experimental reasons. Mathematically, the two symbols are used for distinction in the Abel transform equations. Experimentally, y is used for the optical measurement, and r is used for the calculated physical parameter.

Conversely, the inverse Abel transform is used to calculate the relative refractive index from the measured phase shift:

$$\Delta n(r) = -\frac{\lambda}{2\pi^2}\int_r^\infty \frac{\partial\phi(y)}{\partial y}\frac{1}{\sqrt{y^2 - r^2}}\mathrm{d}y. \tag{2}$$

In practice, the upper integration limit of both equations is set to the maximum radius at which the index needs to be known. For optical fibers this is typically the fiber core radius or the fiber cladding radius. The use of Eq. (2) will only provide the refractive index of the fiber relative to a surrounding medium in which the phase shift is zero. To obtain the absolute refractive index of the fiber, the index of the surrounding medium, n_{med}, must be known. The absolute refractive index can then be calculated using

$$\Delta n(r) = n_{\mathrm{fiber}}(r) - n_{\mathrm{med}}. \tag{3}$$

Typically, a fluid of known refractive index is used to surround the fiber. If only the absolute refractive index of the core is desired, an index matching fluid that matches the cladding refractive index is used.

As with any experimental measurement, the phase-shift measurement will contain noise. The need to numerically differentiate the noisy data in the inverse Abel transform, Eq. (2), leads to large errors in the calculated data [12]. Many early algorithms to compute the transform can be characterized by the use of curve fitting techniques to smooth out the noisy data, thus allowing for analytic differentiation. See [12,13] for a thorough review. Other algorithms were developed that manipulated the inverse Abel transform to remove the derivative [14,15]. However, it was shown that manipulating the transform did not always remove the errors inherent in numerically differentiating the noisy data [16]. Two Fourier-based algorithms were developed in which the measured data were represented as a Fourier cosine series [17,18]. While these algorithms showed improvements over previous algorithms with noiseless data, their performance with noisy data was not reported. Improvements in transforming slightly noisy data were shown with an iterative algorithm [19]. In this algorithm, a scaled version of the noisy data was used as a first approximation of the calculated data and then iteratively improved using further manipulated versions of the noisy data.

In this paper, a direct differentiation algorithm, the iterative algorithm [19], and the more recent of the two Fourier-based algorithms [18] are evaluated.

The direct differentiation algorithm was chosen due to its use of common numerical methods to directly solve the inverse Abel transform as it appears in Eq. (2). The iterative algorithm was chosen for its demonstrated performance on noisy data. The Fourier-based algorithm was chosen due to its use with several of the phase-shift and retardation measurement techniques mentioned previously [3,4,11].

3. Methods

To evaluate the performance of an inverse Abel transform algorithm, five main steps were as follows:

1. A mathematical model was chosen for the model relative refractive-index profile.
2. A model phase-shift profile was calculated analytically using the forward Abel transform of the model index profile.
3. Noise was added to the model phase-shift profile to simulate an experimentally measured, noisy phase-shift profile.
4. The relative refractive index was numerically calculated using the inverse Abel transform algorithm on the noisy phase shift.
5. The performance of the algorithm was quantified by calculating the rms error between the calculated index profile and the model index profile.

A model of a fiber core with a power-law index profile featuring a central dip was chosen as the model index profile [17]. Mathematically, this index profile is given by

$$\Delta n(r) = \Delta n(1 - r^2) - \Delta n D\left(\frac{1}{1 + r^2/W^2} - \frac{1}{1 + 1/W^2}\right), \tag{4}$$

where r is the radial distance from the longitudinal fiber axis, and D and W correspond to the depth and width of the central dip. For this profile, r is normalized to the fiber core radius. For a profile with no central dip, $D = 0$, the parameter Δn corresponds to the maximum index difference between the core and the cladding. For the results presented in this paper, a profile with a moderate central dip ($D = 0.5$, $W = 0.1$, and $\Delta n = 1$) was chosen. This model index profile is shown in Fig. 1.

The model phase-shift profile corresponding to the index profile of Eq. (4) was calculated analytically using the forward Abel transform. The model phase-shift profile resulting from the index profile with a moderate central dip is shown as a solid curve in Fig. 2. As with the index profile, the radial distance from the longitudinal fiber axis, y, is normalized to the fiber core radius.

Noise was added to the model phase-shift profile to simulate an experimental measurement. In practice, the phase-shift profile is extracted from digitally captured transverse images of the fiber. The resolution of the imaging system determines the number of points along the fiber core radius, between $r = 0$ and $r = 1$, over which the phase shift is measured. To simulate a realistic measurement, 50 points were chosen along the fiber core radius for the noisy phase-shift profile. This corresponds to a transverse image of the fiber in which 50 pixels capture the phase-shift profile of the fiber core radius. The noise present in the imaging system determines the level and distribution of noise in the phase-shift measurement. To simulate experimentally observed measurements, Gaussian random noise was added to each point of the model phase shift. The mean of the Gaussian-distributed noise was zero, and the standard deviation was chosen to yield a noisy phase shift with an rms error of 0.03 rad (1.72°) when compared to the model phase shift. This level of noise was chosen to match noise levels observed in phase-shift measurements made using the microinterferometric optical phase tomography (MIOPT) technique [20]. In this technique, the phase-shift measurement is obtained from digital images of the interference fringes produced by the fiber. To reduce noise in the measurement, each image is created by averaging 20 frames from a CCD video camera. A typical noisy phase-shift profile is shown with the dots in Fig. 2.

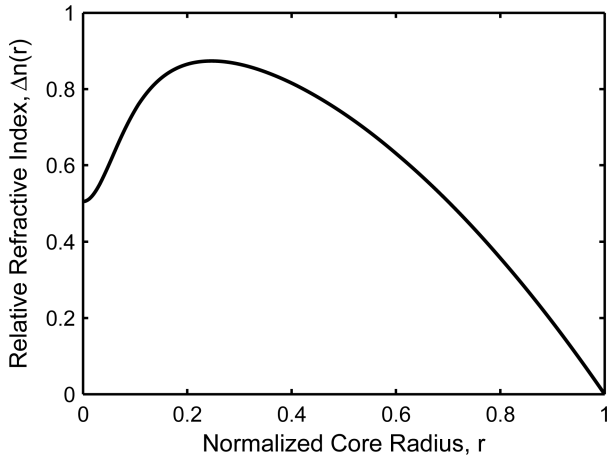

Fig. 1. Model relative refractive-index profile featuring a moderate central dip ($D = 0.5$, $W = 0.1$).

Calculation of the refractive index from the noisy phase shift was performed using each algorithm mentioned in Section 2. Each algorithm featured one or more variable parameters, which were sequentially varied to determine their optimal values. In the direct differentiation algorithm, both the differentiation and integration in the inverse Abel transform were performed numerically. The differentiation was performed using a combination of forward-, central-, and backward-difference approximations. The integration was performed using a trapezoidal approximation. The performance of each approximation, and therefore the algorithm, was affected by the spacing between noisy phase-shift data points. This spacing was varied by changing the number of points along the fiber core radius, N, for the noisy phase shift. Because the original noisy phase shift was generated with 50 points along

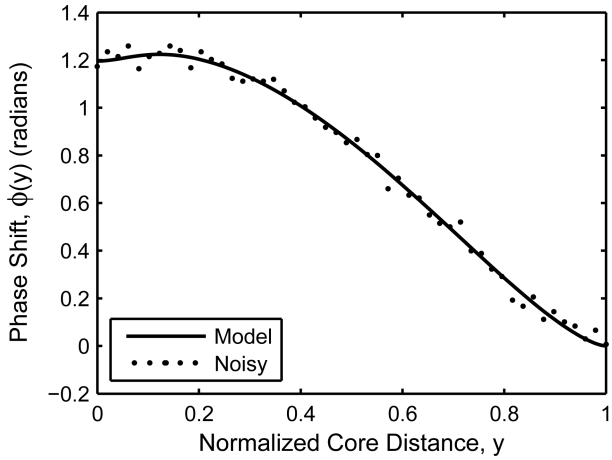

Fig. 2. Model (solid curve) and noisy (dots) phase-shift profiles. The noisy phase shift has an rms error of 0.03 rad (1.72°) when compared to the model phase shift.

the fiber core radius, linear interpolation was used to increase and decrease N.

The iterative algorithm, described in [19], requires numerical integration to be performed over the fiber core radius. Thus, the number of points along the fiber core radius, N, is a parameter when testing this algorithm. The iterative algorithm also requires that an initial approximation of the relative refractive index be iteratively improved. The index profile is first approximated by a scaled version of the noisy phase shift. This initial approximation is then iteratively improved by adding to it a further manipulated version of the noisy phase shift. Therefore, the number of iterations, m, is a second parameter.

The Fourier algorithm, described in [18], requires that the noisy phase-shift data be represented by a Fourier cosine series. Therefore, the first parameter is the number of Fourier harmonics, k. The Fourier algorithm also requires a numerical integration. However, unlike the previous algorithms, the integral is performed over a transformed variable. This introduces the step size of the transformed variable, defined as dt, as a second parameter. The number of points along the fiber core radius, N, also remains a factor in the integration due to the dependence of the transformed variable on the radial distance from the longitudinal fiber axis.

For each algorithm, the parameters were sequentially varied over a range in which the best algorithm performance was observed. For each value of the parameters, the rms error between the calculated index profile and the model index profile was determined. Due to the random nature of noise added in the phase-shift profiles, the performance of the algorithms was found to vary when different noisy phase-shift profiles were used. Therefore, each algorithm was tested with 100 noisy profiles. To judge the overall performance of an algorithm and determine the optimal values of the parameters, the average rms error among all 100 calculated index profiles and the model index profile was determined.

4. Results

As stated in Section 3, the results presented represent the average performance of the algorithms. Therefore, the optimal values for the free parameters are not absolute but rather provide an indication of a small range of the parameters over which calculated index profiles can be qualitatively analyzed. The values given are also for the specific index profile and simulated noise discussed in Section 3. To provide more general results, two steps were taken. First, an index profile with a deeper, more narrow central dip ($D = 1, W = 0.05$) was tested to determine the effect of a more rapidly varying index profile. Second, noisy phase-shift profiles in which the noise was added to 100 points along the fiber core radius were tested for both index profiles. The effects of changing the index profile and the number of points used when adding noise will be discussed for each algorithm.

A. Direct Differentiation Algorithm

The average rms error in the index profiles calculated with the direct differentiation algorithm is shown in Fig. 3. The error is plotted versus the number of points along the fiber core radius, N. The minimum average rms error was 0.11 and occurred for $N = 91$. Also shown in Fig. 3 is the standard deviation of the rms error. At the minimum in average rms error, the standard deviation in rms error was 0.015.

There are two important features illustrated in Fig. 3. First, there is a minimum in the average rms error followed by a steady increase as N is increased. The effect of increasing N is to decrease the spacing between points in the approximation of the derivative. With noiseless data, decreased spacing would lead to a more accurate result. With noisy data however, a smaller spacing results in more noise being added to the result [12]. Second, there is a small increase in the average rms error when N is near a multiple of 50. Recall that 50 points were used in the generation of the noisy phase shift and that

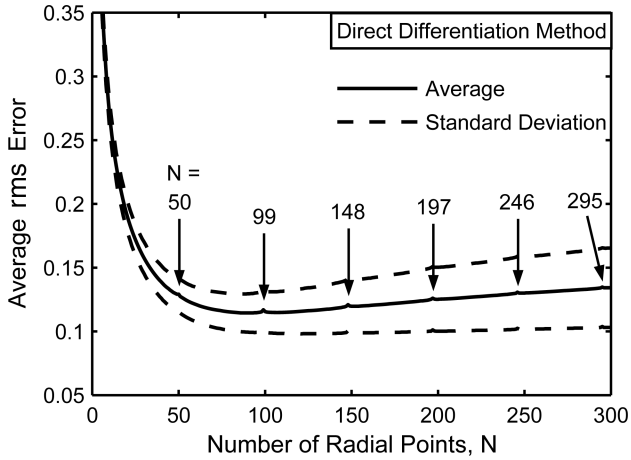

Fig. 3. Average rms error in the index profiles calculated with the direct differentiation algorithm. The minimum average rms error is 0.11 and occurs for $N = 91$. Values of N for which the error spikes due to interpolation effects are indicated.

linear interpolation was used to increase or decrease N. In general, the interpolated data will exactly represent the original noise added if

$$N = (N_0 - 1)i + 1, \tag{5}$$

where N_0 is the number of points used in the generation of the noisy phase shift, and i is a positive integer. For the results shown in Fig. 3, $N_0 = 50$, and thus the interpolated data exactly represents the original noise for values of $N = 50$, 99, 148, 197, 246, and 295. The small spikes in rms error at these values of N are pointed out in Fig. 3. However, when N is not given by Eq. (5), interpolated data points will not match up with the original noise. This leads to a smoothing of the original noise, thus reducing the rms noise of the phase shift and the rms error in the calculated index profile. These features indicate that the optimal value of N for a single noisy phase-shift profile will be $50 < N < 100$, or in general $N_0 < N < 2N_0$.

Qualitatively, the direct differentiation algorithm produced the lowest quality calculated index profiles. The error in the calculated index profiles was often large in some regions and small in others. This is due to the random distribution of noise in the phase-shift profiles. Because the approximation of the derivative works point by point, regions with larger amounts of noise in the phase-shift profiles resulted in regions with larger error in the index profiles. Furthermore, the calculated index profiles were often an underestimate of the model index profiles. A typical calculated index profile illustrating these characteristics is shown by the dots in Fig. 4. The index profile was calculated using $N = 91$.

The performance of the direct differentiation algorithm was similar for the index profile with the deeper, more narrow central dip. For profiles in which the original noisy phase shift was generated with $N_0 = 100$ points along the fiber core radius, the minimum average rms error occurred for values of N near 150. This further supports the general rule of $N_0 < N < 2N_0$.

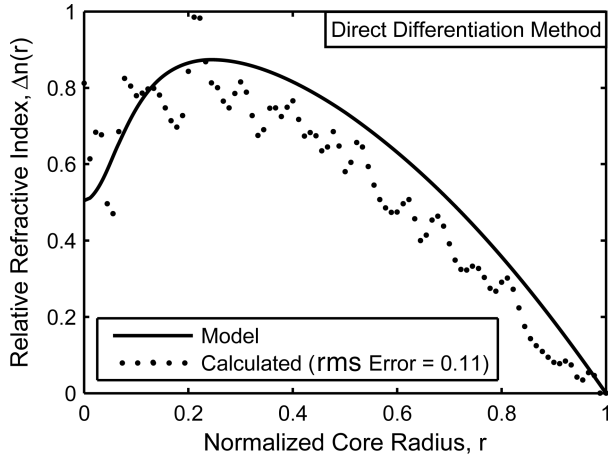

Fig. 4. Typical relative refractive-index profile calculated with the direct differentiation algorithm (dots). Shown for reference is the model index profile (solid curve). The calculated profile illustrates nonuniform distribution of the error and underestimation of the model index profile.

B. Iterative Algorithm

The average rms error in the index profiles calculated with the iterative algorithm is shown in Fig. 5. The error is plotted versus two free parameters: the number of points along the fiber core radius, N, and the number of iterations, m. The minimum average rms error was 0.08 and occurred for $N = 20$ and $m = 6$. The standard deviation in the rms error followed a similar trend to that of the direct differentiation algorithm. For small values of N and m, the standard deviation was low; as N and m increased, the standard deviation increased monotonically. At the minimum, the standard deviation in rms error was 0.014.

There are three important features illustrated in Fig. 5. First, for a constant m, there is an increase in the average rms error when N is near a multiple of 50. This feature is similar to the small increases in error seen with the direct differentiation algorithm and can be explained in the same manner. Second, for a constant value of m, there is a minimum in the average rms error for small values of N. Ignoring the spike in error when $N = 50$, the minimum is followed by a slight increase in error and then a constant error as N increases. For the results shown, the minimum in error occurs near $N = 20$ for most values of m. Qualitatively, this small value of N is too few points to represent the central dip of the index profile. Once N is increased above 40, however, the error remains constant for any further increase in N. These two features indicate that the optimal value of N for a single noisy phase-shift profile will be near, but below, the original number of points used in the generation of the noisy phase shift. In general, N should be near, but below, N_0.

The third important feature in Fig. 5 is that for a constant N, there is a minimum in the average rms error followed by a steady increase as m is increased.

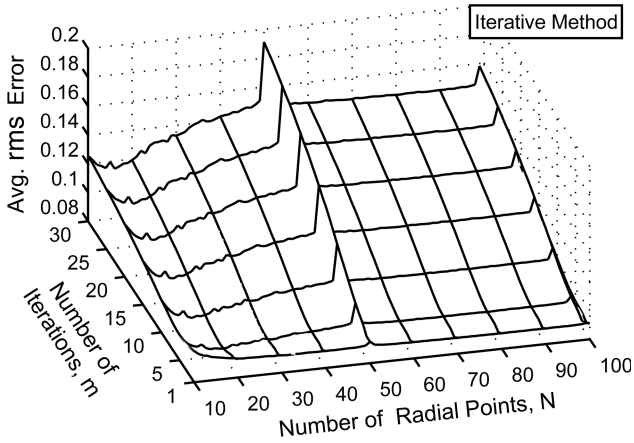

Fig. 5. Average rms error in the index profiles calculated with the iterative algorithm. The minimum average rms error is 0.08 and occurs for $N = 20$ and $m = 6$.

For values of N near the optimal value (40–49), the minimum in average rms error occurs for $m = 2$. The subsequent increase in error with the number of iterations is due to the compounding of the original noise with each successive iteration. As described in Section 3, the index profile was first approximated by a scaled version of the noisy phase shift. This initial approximation was then iteratively improved by adding a further manipulated version of the noisy phase shift to it. Through each iteration the original noise always adds to itself, thus resulting in an index profile with increased rms error. This feature suggests that, for data with noise levels similar to those in the simulated noisy phase shift, very few iterations should be performed.

Qualitatively, the iterative algorithm produced consistent calculated index profiles. The depth of the central dip in the calculated index profiles was underestimated for small values of m. A value of $m > 8$ was typically required to reproduce the depth of the central dip. As previously discussed, using such large values of m resulted in large rms errors in the calculated index profiles. Although the rms error was large, it was distributed much more uniformly than in the case of index profiles calculated using the direct differentiation algorithm. This indicates that the calculated index profiles may be improved using averaging or filtering. A typical calculated index profile illustrating these characteristics is shown by the dots in Fig. 6. The index profile was calculated using $N = 40$ and $m = 6$.

Due to the need for a large number of iterations to accurately represent the central dip, the iterative algorithm produced poor results for the index profile with a deeper, more narrow central dip. Any accuracy gained in the central dip was overshadowed by a large error throughout the index profile. For moderate-dip profiles, in which the original noisy phase shift was generated with $N_0 = 100$ points along the fiber core radius, the general rules for selecting

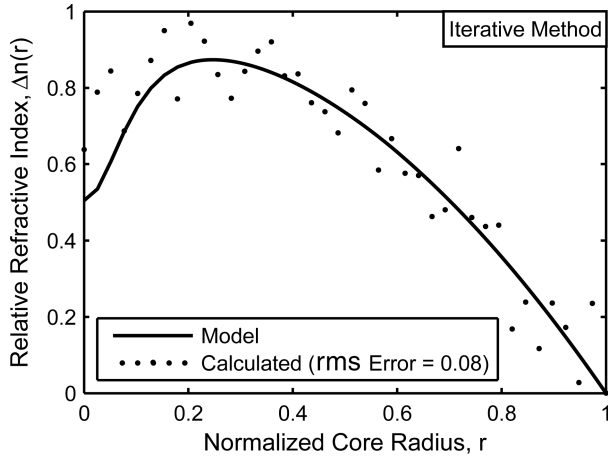

Fig. 6. Typical relative refractive-index profile calculated with the iterative algorithm (dots). Shown for reference is the model index profile (solid curve). The calculated profile illustrates underestimation of the central dip depth and uniform distribution of the error.

N and m remained as previously given. The optimal value of N was near, but below, N_0, and small values of m gave the lowest rms error, while slightly higher values better represented the central dip of the index profile.

C. Fourier Algorithm

The average rms error in the index profiles calculated with the Fourier algorithm is shown in Fig. 7. The error is plotted versus two free parameters: the number of points along the fiber core radius, N, and the number of Fourier harmonics, k. The minimum average rms error was 0.04 and occurred for $N = 81$ and $k = 6$. The standard deviation in the rms error followed a similar trend to that of the previous two algorithms. For small values of N and k, the standard deviation was low; as N and k increased, the standard deviation increased monotonically. At the minimum, the standard deviation in rms error was 0.011.

There are two important features illustrated in Fig. 7. First, the rms error is highly dependent on the choice of k. For constant N, there is a clear minimum in rms error for $k = 6$ followed by a steady increase as k is increased. Furthermore, even values of k generally give better results than odd values. Second, the rms error is affected very little by N. Slightly visible for large values of k is a small increase in the error with $N = 50$. This is consistent with the interpolation effects discussed with the previous two algorithms. However, for values of k near the optimal value, this effect is not seen. For $k = 6$, the difference in the average rms error at $N = 50$ and the minimum rms error is less than 10^{-3}. This means that as long as k is near the optimal value, N can be set equal to the original number of points used in the generation of the noisy phase shift, N_0. This eliminates the need for linear interpolation and simplifies the algorithm.

The Fourier algorithm also had a third free parameter: the step size of the transformed variable, dt. However, it was found that for d$t \le 10^{-2}$, the average rms error in calculated index profiles was practically

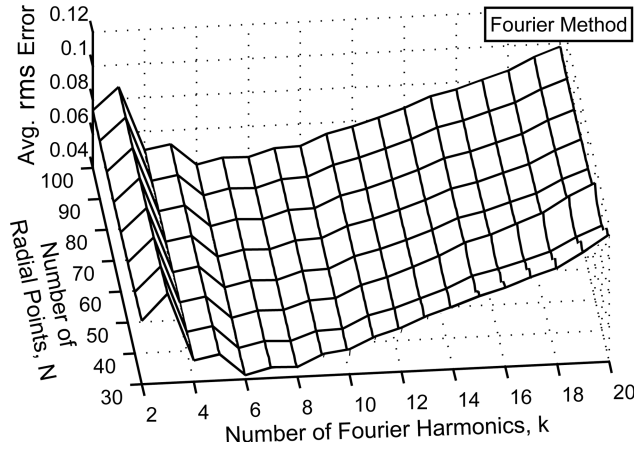

Fig. 7. Average rms error in the index profiles calculated with the Fourier algorithm. The minimum average rms error is 0.04 and occurs for $N = 81$ and $k = 6$.

independent of dt. Because the transformed variable depends on y and r, the step size should be chosen relative to the range covered by y and r. In the cases presented here, y and r each ranged from 0 to 1, and $dt \leq 10^{-2}$. In general, dt should be chosen to be at least one one-hundredth of the range covered by y and r.

Qualitatively, the Fourier algorithm produced the highest quality calculated index profiles. However, there remains a common characteristic in the calculated index profiles that can be misleading. The relatively small number of Fourier harmonics causes the calculated index profile to vary slowly about the model index profile, as is commonly seen with finite Fourier series representations. While this produces index profiles with evidently little noise, the slow variations could be mistaken for features in the actual index profile. This characteristic is illustrated by the calculated index profile shown by the dots in Fig. 8. The index profile was calculated using $N = 50$, $k = 6$, and $dt = 10^{-4}$.

The performance of the Fourier algorithm remained independent of N and dt for the index profile with a deeper, more narrow central dip. However, the optimal value of k approximately doubled to approximately 14 due to the more rapidly varying profile. For profiles in which the original noisy phase shift was generated with $N_0 = 100$ points along the fiber core radius, the average rms error remained independent N. This further supports elimination of linear interpolation to change the number of points along the fiber core radius.

5. Summary and Discussion

The performance of three algorithms for computing the refractive-index profile of optical fibers was both quantitatively and qualitatively evaluated. Quantitatively, the performance of the algorithms was assessed based on the average rms error present in index profiles computed from noisy phase-shift profiles. Qualitatively, the algorithms were evaluated based on features commonly seen in calculated index profiles. Of the three algorithms studied, the Fourier algorithm provided the overall best results. The minimum average rms error for the Fourier algorithm was twice as small as the iterative algorithm and almost three times smaller than the direct differentiation algorithm. Furthermore, the Fourier algorithm allowed for elimination of linear interpolation of the noisy phase shift. This both simplified the algorithm and removed any manipulation of the phase-shift data before it was processed by the algorithm. The disadvantage of the Fourier algorithm was the presence of slowly varying features in the calculated index. These features were due to the small optimal value for the number of Fourier harmonics and could be mistaken for features not present in an actual fiber or fiber device. This effect may be reduced, with a trade-off of increased rms error, by increasing the number of Fourier harmonics. In practice, this decision will require qualitative analysis of calculated index profiles.

The results presented were generated from noisy phase-shift profiles that were developed to simulate experimental data. In practice, however, image processing may be used on the fiber images to reduce the noise further. One common noise-reduction technique is to apply a Weiner filter to the fiber images. To simulate this effect, a Weiner filter was applied directly to the noisy phase-shift profiles. The filtered phase-shift profiles were then tested with the same method that was used on the noisy phase-shift profiles. For each algorithm, the resulting calculated index profiles showed lower rms errors and improved qualitatively. In addition, the relative accuracies of the algorithms remained unchanged. That is, the Fourier algorithm provided the most accurate index profiles, from filtered phase-shift profiles, and the direct differentiation algorithm provided the least accurate profiles.

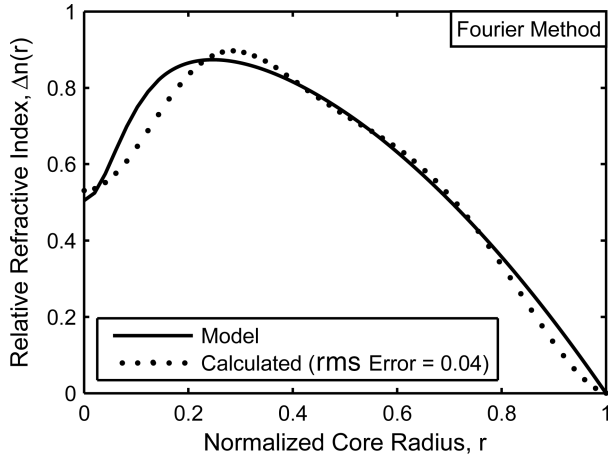

Fig. 8. Typical relative refractive-index profile calculated with the Fourier algorithm (dots). Shown for reference is the model index profile (solid curve). The calculated profile illustrates slow variations that could be mistaken for actual index profile features.

References

1. H. M. Presby, D. Marcuse, H. W. Astle, and L. M. Boggs, "Rapid automatic index profiling of whole-fiber samples. II," Bell Syst. Tech. J. **58**, 883–902 (1979).
2. A. Barty, K. A. Nugent, D. Paganin, and A. Roberts, "Quantitative optical phase microscopy," Opt. Lett. **23**, 817–819 (1998).
3. A. Roberts, E. Ampem-Lassen, A. Barty, K. A. Nugent, G. W. Baxter, N. M. Dragomir, and S. T. Huntington, "Refractive-index profiling of optical fibers with axial symmetry by use of quantitative phase microscopy," Opt. Lett. **27**, 2061–2063 (2002).
4. E. Ampem-Lassen, S. T. Huntington, N. M. Dragomir, K. A. Nugent, and A. Roberts, "Refractive index profiling of axially symmetric optical fibers: a new technique," Opt. Express **13**, 3277–3282 (2005).
5. N. M. Dragomir, E. Ampem-Lassen, S. T. Huntington, G. W. Baxter, A. Roberts, and P. M. Farrell, "Refractive index profiling of optical fibers using differential interference contrast microscopy," IEEE Photon. Technol. Lett. **17**, 2149–2151 (2005).
6. P. L. Chu and T. Whitbread, "Measurement of stresses in optical fiber and preform," Appl. Opt. **21**, 4241–4245 (1982).

7. C. C. Montarou, T. K. Gaylord, B. L. Bachim, A. I. Dachevski, and A. Agarwal, "Two-wave-plate compensator method for full-field retardation measurements," Appl. Opt. **45**, 271–280 (2006).
8. K. W. Raine, R. Feced, S. E. Kanellopoulos, and V. A. Handerek, "Measurement of axial stress at high spatial resolution in ultraviolet-exposed fibers," Appl. Opt. **38**, 1086–1095 (1999).
9. Y. Park, T.-J. Ahn, Y. H. Kim, W.-T. Han, U. C. Paek, and D. Y. Kim, "Measurement method for profiling the residual stress and the strain-optic coefficient of an optical fiber," Appl. Opt. **41**, 21–26 (2002).
10. Y. Park, S. Choi, U.-C. Paek, K. Oh, and D. Y. Kim, "Measurement method for profiling the residual stress of an optical fiber: detailed analysis of off-focusing and beam-deflection effects," Appl. Opt. **42**, 1182–1190 (2003).
11. C. C. Montarou, T. K. Gaylord, and A. I. Dachevski, "Residual stress profiles in optical fibers determined by the two-waveplate-compensator method," Opt. Commun. **265**, 29–32 (2006).
12. E. W. Hansen and P. L. Law, "Recursive methods for computing the Abel transform and its inverse," J. Opt. Soc. Am. A **2**, 510–520 (1985).
13. C. J. Cremers and R. C. Birkebak, "Application of the Abel integral equation to spectrographic data," Appl. Opt. **5**, 1057–1064 (1966).
14. C. K. Chan and P. Lu, "On the stability of the solution of Abel's integral equation," J. Phys. A **14**, 575–578 (1981).
15. M. Deutsch and I. Beniaminy, "Derivative-free inversion of Abel's integral equation," Appl. Phys. Lett. **41**, 27–28 (1982).
16. R. S. Anderssen and F. R. de Hoog, "On the method of Chan and Lu for Abel's integral equation," J. Phys. A **14**, 3117–3121 (1981).
17. K. Tatekura, "Determination of the index profile of optical fibers from transverse interferograms using Fourier theory," Appl. Opt. **22**, 460–463 (1983).
18. M. Kalal and K. A. Nugent, "Abel inversion using fast Fourier transforms," Appl. Opt. **27**, 1956–1959 (1988).
19. P. A. Vicharelli and W. P. Lapatovich, "Iterative method for computing the inverse Abel transform," Appl. Phys. Lett. **50**, 557–559 (1987).
20. B. L. Bachim, T. K. Gaylord, and S. C. Mettler, "Refractive-index profiling of azimuthally asymmetric optical fibers by microinterferometic optical phase tomography," Opt. Lett. **30**, 1126–1128 (2005).